ACS Sustainable Chemistry & Engineering

pubs.acs.org/journal/ascecg

Research Article

Kinetic Model for the Direct Conversion of CO_2/CO into Light Olefins over an In_2O_3–ZrO_2/SAPO-34 Tandem Catalyst

Ander Portillo, Onintze Parra, Andres T. Aguayo, Javier Ereña, Javier Bilbao, and Ainara Ateka*

Cite This: *ACS Sustainable Chem. Eng.* 2024, 12, 1616–1624

Read Online

ACCESS | Metrics & More | Article Recommendations | Supporting Information

ABSTRACT: An original kinetic model is proposed for the direct production of light olefins by hydrogenation of CO_2/CO (CO_x) mixtures over an In_2O_3–ZrO_2/SAPO-34 tandem catalyst, quantifying deactivation by coke. The reaction network comprises 12 individual reactions, and deactivation is quantified with expressions dependent on the concentration of methanol (as coke precursor) and H_2O and H_2 (as agents attenuating coke formation). The experimental results were obtained in a fixed-bed reactor under the following conditions: In_2O_3–ZrO_2/SAPO-34 mass ratio, 0/1–1/0; 350–425 °C; 20–50 bar; H_2/CO_x ratio, 1–3; CO_2/CO_x ratio, 0–1; space time, 0–10 $g_{In2O3-ZrO2}$ h mol_C^{-1}, 0–20 $g_{SAPO-34}$ h mol_C^{-1}; time, up to 500 h; H_2O and CH_3OH in the feed, up to 5% vol. The utility of the model for further scale-up studies is demonstrated by its application in optimizing the process variables (temperature, pressure, and CO_2/CO_x ratio). The model predicts an olefin yield higher than 7% (selectivity above 60%), a CO_x conversion of 12% and a CO_2 conversion of 16% at 415 °C and 50 bar, for a CO_2/CO_x = 0.5 in the feed. Additionally, an analysis of the effect of In_2O_3–ZrO_2 and SAPO-34 loading in the configuration of the tandem catalyst is conducted, yielding 17% olefins and complete conversion of CO_2 under full water removal conditions.

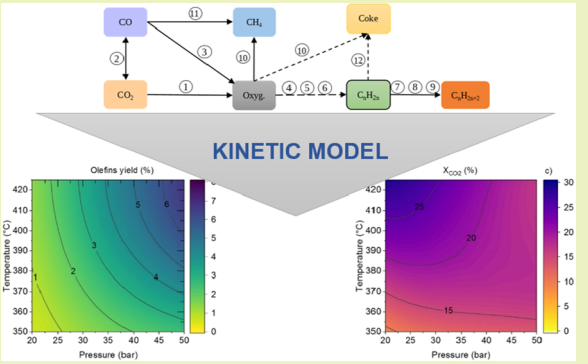

KEYWORDS: *kinetic model, deactivation, CO_2 valorization, olefins, In_2O_3–ZrO_2, SAPO-34, tandem catalyst*

INTRODUCTION

The processes for the direct production of fuels and chemicals by hydrogenation of CO_2, such as the modified Fischer–Tropsch (MFT)[1] and oxygenates (methanol/dimethyl ether (DME)) intermediated routes,[2] are particularly attractive within the framework of Carbon Capture Utilization and Sequestration (CCUS) strategies.[3] The route proceeding via oxygenates as intermediates requires OX/ZEO (metallic oxide/zeotype) tandem catalysts[4] and enables the selective production of olefins,[5] paraffins,[6] aromatics,[7,8] or C_{5+} hydrocarbons suitable for use as gasoline[9,10] by selecting a zeotype with appropriate acidity and shape selectivity. A notable advantage of this process compared to the two-stage synthesis of methanol and subsequent conversion to hydrocarbons is that the *in situ* conversion of methanol/DME to hydrocarbons shifts the thermodynamic equilibrium of methanol synthesis.[11]

The processes of methanol/DME synthesis from CO_2 and the conversion of oxygenates to hydrocarbons have reached considerable level and technological development.[12−17] Similarly, the conversion of methanol to hydrocarbons has also progressed.[18−23] However, the optimal conditions for the integrated process differ from those of the individual reaction stages. Moreover, the composition of the reaction medium is also different. Consequently, OX/ZEO tandem catalysts with different configurations, activities, selectivities, and stabilities have been designed for the specific reaction conditions of the integrated process.[24]

In previous studies, the excellent performance of the In_2O_3–ZrO_2/SAPO-34 tandem catalyst for the selective production of light olefins was examined,[25] based on the synergy between the CO_2 adsorption capacity and hydrogenation activity of the oxygen vacancies on the In_2O_3–ZrO_2 catalyst surface,[26] and on the characteristic olefin selectivity of the CHA (Chabazite) structure of SAPO-34.[27] Additionally, the ability of this catalyst to simultaneously convert CO_2 and CO facilitates the cofeeding of syngas with CO_2, which contributes to the sustainability process (when syngas is obtained from biomass or waste of the consumer society) and provides part of the required green H_2. The negative synergistic effects of excessive concentration of H_2O and methanol in the medium of the integrated process have also been studied. Particularly the features regarding the deactivation of the tandem catalyst, which affects the reaction conditions,[28] the configuration of the

Received: October 23, 2023
Revised: January 4, 2024
Accepted: January 5, 2024
Published: January 18, 2024

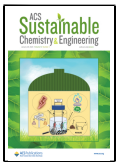

tandem catalyst (OX/ZEO ratio), and the arrangement in the reactor, which must be appropriate to mitigate deactivation.[29]

In this paper, an original kinetic model has been established, which is essential for the scale-up of the process. Note that previous studies on the kinetic modeling of the direct synthesis of hydrocarbons from CO_2 over tandem catalysts are scarce. Ghosh et al.[30] proposed a kinetic model for the conversion of CO_2 to a broad range of hydrocarbons (C_2−C_{9+}, including aromatics) over an In_2O_3/HZSM-5 tandem catalyst. The reaction network consists of 21 elementary steps (simplified to 11), considering the reactions catalyzed by the In_2O_3 and the HZSM-5 catalysts. The rate kinetic equations follow a Langmuir−Hinshelwood (LH) type, including terms that quantify the extent of reaction limitation by reactant adsorption on the active sites of each individual catalyst. To simplify the calculation of the kinetic parameters, previously obtained for the reactions involved in methanol synthesis catalyzed by In_2O_3[31] were used and those for the reactions activated by HZSM-5 zeolite were calculated. Cordero−Lanzac et al.[32] established a kinetic model for the direct formation of C_2−C_4 paraffins from CO_2/CO over a $PdZn/ZrO_2$ + SAPO-34 tandem catalyst. The reaction network consists of seven reaction steps, considering the reactions activated by the $PdZn/ZrO_2$ catalyst (methanol synthesis from CO_2, reverse Water Gas Shift (rWGS), methanation, and formation of each C_2−C_4 paraffin from methanol). In this model, the expressions of the reaction rates follow LH-type equations and quantify the limitations of the reaction extent due to reactant and H_2O adsorption. It is noteworthy that these kinetic models in the literature[30,32] do not consider catalyst deactivation, nor the cofeeding of CO, which are original aspects considered in this manuscript. The applicability of the model to tandem catalysts with different loadings of In_2O_3−ZrO_2 and SAPO-34 is also an original contribution. The versatility of the kinetic model is demonstrated by applying it to analyze the effect of reaction variables, such as pressure, temperature, and space time of each individual catalyst, while also considering the cofeeding of CO along with CO_2.

EXPERIMENTAL SECTION

Tandem catalysts were obtained by physically mixing the In_2O_3−ZrO_2 and SAPO-34 (ACS Material) catalysts with particle sizes in the range of 125−250 and 300−400 μm, respectively. The preparation of In_2O_3−ZrO_2 was previously described in detail elsewhere by Portillo et al.[26] Briefly, a coprecipitation using $In(NO_3)_3$ (Sigma-Aldrich), $Zr(NO_3)_4$ (Panreac), and NH_4CO_3 (Panreac) was carried out. The fresh and deactivated catalysts were extensively characterized in previous studies,[26,27] and their properties are presented in Section S1 (Table S1).

The kinetic runs were conducted using a PID Eng. & Tech. Microactivity Reference reactor setup, as detailed in Portillo et al.,[25] employing an isothermal fixed-bed reactor under a wide range of operating conditions: In_2O_3−ZrO_2/SAPO-34 mass ratio, 0/1−1/0; 350−425 °C; 20−50 bar; H_2/CO_x molar ratio in the feed, 1−3; CO_2/CO_x molar ratio in the feed, 0−1; space time (defined as the ratio between the mass of each individual catalyst and the molar flow of CO_2/CO at the reactor inlet), 0−10 $g_{In2O3-ZrO2}$ h mol_C^{-1}, 0−20 $g_{SAPO-34}$ h mol_C^{-1}; time on stream, up to 500 h; H_2O and CH_3OH in the feed, up to 5% vol. For the analysis of the composition of the feed and product streams, a Varian CP-4900 (Agilent) microchromatograph was used, as described by Portillo et al.[25]

In Section S2, Table S2 specifies the conditions used for each experimental run considered for the modeling. Note that several runs were repeated to ascertain the reproducibility of the experiment. As an example of the reproducibility of the runs, the results of three reactions carried out at certain conditions are displayed in Figure S1. Moreover, the absence of mass transfer constraints for the catalysts was ascertained in Section S3, both theoretically, according to the compliance with the Weisz−Prater criteria (eq S1) for the internal diffusion, and also experimentally, as illustrated in Figures S2 and S3, for internal and external diffusion, respectively.

The modeling was carried out fitting the molar fractions of the components, and the simulation results were quantified by calculating olefin yields, Y_i (eq S2), CO_2 conversion, X_{CO2} (eq S3), and CO_x conversion, X_{COx} (eq S4) based on the molar flows of the reactants and products in C content units as defined in Section S4.

RESULTS AND DISCUSSION

Reaction Network. The reaction network, as illustrated in Figure 1, gathers the reactions outlined in Table 1. The

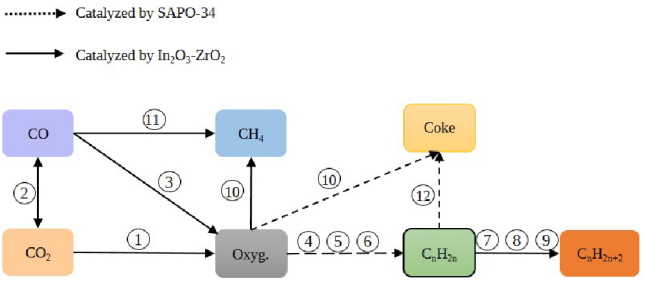

Figure 1. Proposed reaction network. The numbers correspond to the individual reactions in Table 1.

In_2O_3−ZrO_2 catalyzes the methanol synthesis (steps 1, 3; eqs 1 and 3), reverse Water Gas Shift (rWGS) (eq 2), hydrogenation of olefins to paraffins (steps 7−9; eqs 7−9), and methanation (step 11, eq 11) reactions. On the other hand, SAPO-34 catalyzes the formation of olefins from methanol/DME, as described in steps 4−6 (eqs 4−6), with methanol as the reactant, considering DME as an intermediate given its more reactive nature.[33] The decomposition (thermal cracking) of oxygenates (step 10; eq 10), contributes to the formation of CH_4. The reaction network also incorporates the pathways for coke formation, including the decomposition of oxygenates (step 10, eq 10) and the dehydrocyclization of olefins, leading to the formation of aromatics as intermediates, which subsequently condense into polyaromatic species.[34]

Kinetic Equations. The expressions for the kinetics reaction rates are described in Table 1 (eqs 13−23) along with the corresponding individual reaction. The terms θ_{InZr} and $\theta_{SAPO-34}$ consider that the extent of the individual reactions in Table 1 catalyzed by In_2O_3−ZrO_2 and SAPO-34 catalysts, respectively, is limited by the competitive adsorption of different components in the reaction medium on the active sites. This leads to the formulation of a Langmuir−Hinshelwood (LH)-type kinetic model. The best fit of the kinetic model was determined with the following expressions (eqs 24 and 25). Cordero−Lanzac et al.[32] justify the expressions in eqs 24 and 25 by emphasizing the reaction mechanisms and the role of CO_2 and H_2 adsorption as rate-limiting steps in methanol synthesis, as well as the role of H_2O adsorption in limiting SAPO-34 activity in the conversion of oxygenates to olefins.

$$\theta_{InZr} = \frac{1}{(1 + K_{CO_2}^{InZr} P_{CO_2} + (K_{H_2}^{InZr} P_{H_2})^{1/2})^2} \quad (24)$$

https://doi.org/10.1021/acssuschemeng.3c06914
ACS Sustainable Chem. Eng. 2024, 12, 1616−1624

Table 1. Individual Reactions Involved in the Reaction Network of Figure 1 and Corresponding Kinetic Equations

reaction	kinetic equation
$CO_2 + 3H_2 \overset{1}{\leftrightarrow} CH_3OH + H_2O$ (1)	$r_1 = k_1\left(P_{CO_2}P_{H_2}^3 - \frac{P_{CH_3OH}P_{H_2O}}{K_1}\right)\cdot\theta_{InZr}\cdot a_{InZr}$ (13)
$CO_2 + H_2 \overset{2}{\leftrightarrow} CO + H_2O$ (2)	$r_2 = k_2\left(P_{CO_2}P_{H_2} - \frac{P_{CO}P_{H_2O}}{K_2}\right)\cdot\theta_{InZr}\cdot a_{InZr}$ (14)
$CO + 2H_2 \overset{3}{\leftrightarrow} CH_3OH$ (3)	$r_3 = k_3\left(P_{CO}P_{H_2}^2 - \frac{P_{CH_3OH}}{K_3}\right)\cdot\theta_{InZr}\cdot a_{InZr}$ (15)
$2CH_3OH \overset{4}{\rightarrow} C_2H_4 + 2H_2O$ (4)	$r_4 = k_4\cdot P_{CH_3OH}\cdot\theta_{SAPO-34}\cdot a_{SAPO-34}$ (16)
$3CH_3OH \overset{5}{\rightarrow} C_3H_6 + 3H_2O$ (5)	$r_5 = k_5\cdot P_{CH_3OH}\cdot\theta_{SAPO-34}\cdot a_{SAPO-34}$ (17)
$4CH_3OH \overset{6}{\rightarrow} C_4H_8 + 4H_2O$ (6)	$r_6 = k_6\cdot P_{CH_3OH}\cdot\theta_{SAPO-34}\cdot a_{SAPO-34}$ (18)
$C_2H_4 + H_2 \overset{7}{\rightarrow} C_2H_6$ (7)	$r_7 = k_7\cdot P_{C_2H_4}P_{H_2}\cdot\theta_{InZr}\cdot a_{InZr}$ (19)
$C_3H_6 + H_2 \overset{8}{\rightarrow} C_3H_8$ (8)	$r_8 = k_8\cdot P_{C_3H_6}P_{H_2}\cdot\theta_{InZr}\cdot a_{InZr}$ (20)
$C_4H_8 + H_2 \overset{9}{\rightarrow} C_4H_{10}$ (9)	$r_9 = k_9\cdot P_{C_4H_8}P_{H_2}\cdot\theta_{InZr}\cdot a_{InZr}$ (21)
$mCH_3OCH_3 \overset{10}{\rightarrow} mCO + pCO_2 + qH_2 + rCH_4 + sH_2O + xC\ (coke)$ (10)	$r_{10} = k_{10}\cdot P_{CH_3OH}P_{H_2}\cdot\theta_{InZr}$ (22)
$CO + 3H_2 \overset{11}{\leftrightarrow} CH_4 + H_2O$ (11)	$r_{11} = k_{11}\cdot P_{CO}P_{H_2}^3\cdot\theta_{InZr}$ (23)
$C_nH_{2n} \overset{12}{\leftrightarrow} nC\ (coke) + nH_2$ (12)	

Table 2. Parameters of the Kinetic Model (Units at the End)[a]

	Apparent kinetic parameters[b]	
	k_j*	E
k_2	$4.0 \times 10^{-2} \pm 7.0 \times 10^{-4}$	$8.1 \times 10^{0} \pm 1.2 \times 10^{0}$
k_3	$2.3 \times 10^{-5} \pm 5.2 \times 10^{-7}$	$1.8 \times 10^{0} \pm 4.0 \times 10^{-2}$ (same for k_1)
k_5	$3.6 \times 10^{0} \pm 4.9 \times 10^{-4}$	$7.2 \times 10^{0} \pm 1.9 \times 10^{0}$ (same for k_4 and k_6)
k_8	$7.4 \times 10^{-2} \pm 1.5 \times 10^{-3}$	$7.3 \times 10^{-2} \pm 6.1 \times 10^{-4}$ (same for k_7 and k_9)
k_{10}	$1.7 \times 10^{-2} \pm 7.2 \times 10^{-4}$	$9.2 \times 10^{1} \pm 1.5 \times 10^{1}$
	Apparent adsorption parameters	
	K*$_{ads}$	ΔH
$K_{CO_2}^{InZr}$	$5.1 \times 10^{0} \pm 5.9 \times 10^{-1}$	$-5.1 \times 10^{0} \pm 9.6 \times 10^{-1}$
$K_{H_2}^{InZr}$	$7.6 \times 10^{-3} \pm 4.3 \times 10^{-4}$	$-1.7 \times 10^{2} \pm 3.8 \times 10^{0}$
$K_{H_2O}^{SAPO-34}$	$3.1 \times 10^{-4} \pm 7.4 \times 10^{-5}$	$-9.4 \times 10^{-1} \pm 2.9 \times 10^{-1}$
	Apparent deactivation parameters	
	k*$_{d,j}$	E_d
$k_{d,InZr}$	$5.7 \times 10^{-3} \pm 1.7 \times 10^{-3}$	$2.0 \times 10^{0} \pm 6.4 \times 10^{-2}$
$k_{d,SAPO-34}$	$5.7 \times 10^{3} \pm 2.5 \times 10^{2}$	$1.4 \times 10^{-2} \pm 5.0 \times 10^{-3}$
	Apparent adsorption parameters for deactivation	
K_{d,H_2O}^{InZr}	$4.1 \times 10^{-2} \pm 4.2 \times 10^{-4}$	$-2.7 \times 10^{2} \pm 8.2 \times 10^{1}$
K_{d,H_2}^{InZr}	$4.2 \times 10^{-3} \pm 1.0 \times 10^{-3}$	$-4.0 \times 10^{1} \pm 9.8\ 10^{0}$
$K_{d,H_2O}^{SAPO-34}$	$6.8 \times 10^{-3} \pm 1.3 \times 10^{-3}$	$-4.2 \times 10^{0} \pm 9.1 \times 10^{-2}$
$K_{d,H_2}^{SAPO-34}$	$2.8 \times 10^{-4} \pm 1.1 \times 10^{-4}$	$-1.3 \times 10^{1} \pm 2.8 \times 10^{0}$
	Deactivation order	
d_{InZr}		$1.2 \pm 1.7 \times 10^{-2}$
$d_{SAPO-34}$		$2.6 \pm 1.5 \times 10^{-2}$

[a]Units: $k_{1,11}$: $mol_C\ g^{-1}\ h^{-1}\ bar^{-4}$; $k_{2,8}$: $mol_C\ g^{-1}\ h^{-1}\ bar^{-2}$; $k_{3,7,9,10}$: $mol_C\ g^{-1}\ h^{-1}\ bar^{-3}$; $k_{4-6,d}$: $mol_C\ g^{-1}\ h^{-1}\ bar^{-1}$; E_a, ΔH, E_d: kJ mol^{-1}; K: bar^{-1}. [b]Note: $k_1 = 0.01\ k_3$; $k_4 = 0.36\ k_5$; $k_6 = 0.30\ k_5$; $k_7 = 0.36\ k_8$; $k_9 = 0.11\ k_8$; $k_{11} = 10^{-5}\ k_{10}$

$$\theta_{SAPO-34} = \frac{1}{1 + K_{H_2O}^{SAPO-34}P_{H_2O}} \quad (25)$$

The deactivation of each catalyst by coke in the tandem catalyst is considered in eqs 13−21 and 23 with two activity terms, a_{InZr} and $a_{SAPO-34}$, corresponding to the In_2O_3−ZrO_2 and SAPO-34 catalysts, respectively. These terms are defined as reaction rate ratios, as defined by Levenspiel et al.,[35] and are calculated as described by Cordero−Lanzac et al.[36] to take into account the *past history* of the catalyst. The deactivation kinetic

https://doi.org/10.1021/acssuschemeng.3c06914
ACS Sustainable Chem. Eng. 2024, 12, 1616−1624

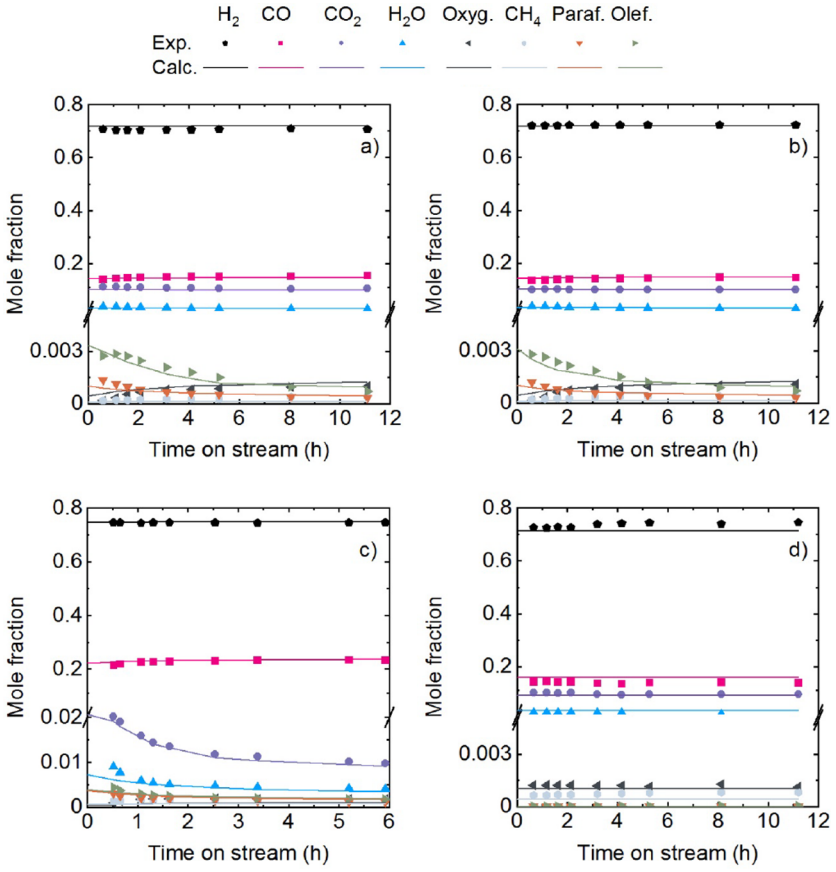

Figure 2. Evolution of product molar fractions with time on stream for the experimental data and calculated values. Reaction conditions: 400 °C; 30 bar; H_2/CO_x ratio in the feed, 3; CO_2/CO_x ratio in the feed, 0.5; space time, 5 g_{cat} h mol_C^{-1}; In_2O_3−ZrO_2/SAPO-34, 2/1 (a). 375 °C; 30 bar; H_2/CO_x ratio in the feed, 3; CO_2/CO_x ratio in the feed, 0.5; space time, 5 g_{cat} h mol_C^{-1}; and In_2O_3−ZrO_2/SAPO-34, 2/1 (b). 400 °C; 50 bar; H_2/CO_x ratio in the feed, 3; CO_2/CO_x ratio in the feed, 0.5; space time, 6.67 g_{cat} h mol_C^{-1}; and In_2O_3−ZrO_2/SAPO-34, 2/2 (c). 400 °C; 30 bar; H_2/CO_x ratio in the feed, 3; CO_2/CO_x ratio in the feed, 0.5; space time, 3.33 g_{cat} h mol_C^{-1}; and In_2O_3−ZrO_2/SAPO-34, 2/0 (d).

expressions are dependent on the concentration of methanol, which is the main precursor of coke:

$$-\frac{da_{InZr}}{dt} = k_{d,InZr}\cdot P_{CH_3OH}\cdot\theta_{d,InZr}\cdot a_{InZr}^{d_{InZr}} \quad (26)$$

$$-\frac{da_{SAPO-34}}{dt} = k_{d,SAPO-34}\cdot P_{CH_3OH}\cdot\theta_{d,SAPO-34}\cdot a_{SAPO-34}^{d_{SAPO-34}} \quad (27)$$

In these equations, the terms $\theta_{d,IZr}$ and $\theta_{d,SAPO\text{-}34}$ quantify the limitation of the extent of coke formation reactions on the In_2O_3−ZrO_2 and SAPO-34 catalysts, respectively, due to the presence of H_2O and H_2, as described by the following expressions:

$$\theta_{d,InZr} = \frac{1}{(1 + K_{d,H_2O}^{InZr}P_{H_2O} + (K_{d,H_2}^{InZr}P_{H_2})^{1/2})^2} \quad (28)$$

$$\theta_{d,SAPO-34} = \frac{1}{(1 + K_{d,H_2O}^{SAPO-34}P_{H_2O} + (K_{d,H_2}^{SAPO-34}P_{H_2})^{1/2})^2} \quad (29)$$

Eqs 26 and 27, along with their complementary counterparts, eqs 28 and 29, align with the results of coke deposition determined in a previous study through TPO analysis of the two catalysts employed under different conditions.[28] Notable findings from these results include: (i) higher coke deposition in SAPO-34; (ii) the influence of methanol concentration favoring coke formation, while H_2O mitigates this formation; and (iii) the converging trend of coke content evolution over time on stream toward a limiting value.

Moreover, it must be mentioned that the role of H_2O[28,37−40] and H_2[29,41−43] as mitigating agents of coke deposition in the conversion of methanol/DME over acid catalysts is well established. Presumably, the role of H_2O in attenuating the condensation of coke intermediates, and of H_2 in facilitating their hydrogenation, will be similar for the coke deposited on the In_2O_3−ZrO_2 catalyst, thereby mitigating its deactivation.

In the calculations, temperature-dependent equilibrium constants for methanol synthesis reactions (steps 1 and 3 in Figure 1) and rWGS (step 2) were used, as proposed by Ateka et al.[12] These expressions were calculated from standard values of formation enthalpies and entropies for the components of each individual reaction.[44]

The mathematical approach used for analyzing the kinetic data in this study has been described in other catalytic processes,[36,45,46] and briefly in Section S5.

Fitting of the Model and Apparent Kinetic Parameters. To evaluate the strong agreement between the calculated molar fractions of the components in the outlet stream of the reactor and the corresponding experimental data, parity plots are presented in Figure S4 (Section S6). The quality of the fit between the calculated and experimental results falls within the typical ranges found in the literature for kinetic models of

https://doi.org/10.1021/acssuschemeng.3c06914
ACS Sustainable Chem. Eng. 2024, 12, 1616−1624

other catalytic processes with complex reaction schemes that consider catalyst deactivation.[36,47−49]

The values of the apparent kinetic parameters resulting in the best fit (with a minimal error objective function, eq S6, corresponding to a confidence degree of 95%) are presented in Table 2. The model simplification study (based on the significance test explained in Section S5), verified that the fit did not improve using different apparent activation energies for the conversion of CO_2 and CO into methanol (steps 1 and 3, respectively, in Figure 1). This lack of improvement may be attributed to their relationship through the rWGS reaction (step 2). Similarly, there was no significant enhancement in the model fit when considering different apparent activation energies in the individual formation of olefins (steps 4−6) and paraffins (steps 7−9), and in the formation of CH_4 through decomposition of methanol (step 10) and oxygenates (step 11). Consequently, the kinetic constants for these steps with the same apparent activation energies are expressed in Table 2 relative to the highest value within the group of reactions sharing the same activation energy. Additionally, constants with the same activation energy are specified at the bottom of the Table 2.

Further comparing the values in Table 2, the apparent constant related to the formation of oxygenates from CO_2 is even 100 times lower than that corresponding to the formation from CO (k^*_3 = 2.3 × 10^{-5} mol_C g^{-1} bar^{-3}). This result confirms that methanol formation reaction will be the key conditioning factor in the extent of the process and that the rWGS reaction plays a crucial role in converting the CO_2/CO mixture into oxygenates, as established in the literature.[11]

Comparing the apparent activation energy values of each reaction, the highest value (92.5 kJ mol^{-1}) corresponds to CH_4 and coke formation from oxygenates (E_{10}), which is in line with the thermal nature of this reaction, that requires temperature control to minimize its extent. The low apparent activation energy values in deactivation kinetics can be justified in catalytic processes involving coke deactivation, where the coke formation/elimination mechanism is complex, and reaction temperature has different effects in reactions of oligomerization, cyclization, dehydrogenation, cracking, etc., justify the apparent activation energy.[50,51]

The remarkable difference between the deactivation constant of SAPO-34 at the reference temperature (5.7 × 10^3 mol_C g^{-1} bar^{-1}) and the negligible value for the In_2O_3−ZrO_2 catalyst (5.7 × 10^{-3} mol_C g^{-1} bar^{-1}) is consistent with previously reported coke deposition results in both catalysts.[28] Moreover, comparing the effect of H_2O adsorption on olefin formation reactions: ($K_{H_2O}^{SAPO-34}$= 3.1 × 10^{-4} bar^{-1}) and deactivation of SAPO-34 ($K_{d,H_2O}^{SAPO-34}$= 6.8 × 10^{-3} bar^{-1}), it is observed that the presence of H_2O offers more advantages (referred to deactivation attenuation) than disadvantages (attenuation of olefin formation). The deactivation kinetics order for the In_2O_3−ZrO_2 catalyst (1.2) indicates an almost linear dependence of the deactivation rate on the remnant activity in eq 26. However, the deactivation order for SAPO−34 in eq 27 is 2.6, indicating a deactivation mechanism with rapid pore blockage by coke deposition, which is typical for this catalyst in the conversion of oxygenates to olefins,[52−54] but maintaining a remnant activity. This tendency is in good agreement with the evolution of coke deposition over time on stream.[28]

Figure S5 displays a covariance matrix relating the kinetic parameters at reference temperature. These information ascertained there is not significant codependence between steps in the reaction mechanism apart from those already considered (correlation between the olefin formation steps 4−6; the steps of paraffin formation 7−9, and the two steps of methanol formation, thus, the formation from CO_2 (step 1) and the formation from CO (step 3)).

To evaluate the adequacy of fitting of the main lumps' evolution over time on stream, Figure 2 shows the molar fractions at the reactor outlet stream, comparing calculated values (lines) with experimental data (points). Challenging conditions with high catalyst deactivation were selected as examples. Figure 2a,b differ in reaction temperature of 400 and 375 °C, respectively. Figure 2c represents a different configuration of the tandem catalyst (In_2O_3−ZrO_2/SAPO−34 mass ratio of 1/1 instead of 2/1 in previous cases) and a higher pressure (50 bar instead of 30 bar). Figure 2d differs in the catalyst (no presence of SAPO−34) and space time (lower) compared with the conditions in Figure 2a. The comparison between calculated and experimental results demonstrates the model's ability to predict the performance under different conditions. Additionally, the model satisfactorily predicts the individual behavior of each catalyst in the tandem system and the impact of the presence of an additional SAPO-34 catalyst. It is observed in Figure 2a−c, that the presence of SAPO-34 is necessary for olefin formation, but rapid deactivation leads to significant composition changes over time on stream. Both Figure 2a,b (with little difference but slightly higher olefin yield at zero time on stream at 400 °C) show a decay in olefin and paraffin concentrations over time, whereas the concentrations of oxygenates (methanol) and CH_4 (very low concentration) increase. The deactivation kinetic model for SAPO-34 (with a deactivation order $d_{SAPO-34}$ of 2.6) predicts, in these figures, a tendency toward constant values over time on stream for the concentrations of olefins, paraffins, and oxygenates.

As mentioned before, the model predicts the complex effects of the catalyst configuration. Figure 2c illustrates the results for a tandem catalyst with a higher SAPO-34 content (In_2O_3−ZrO_2 to SAPO-34 ratio of 2/2). For this configuration, the model predicts two phenomena that have been experimentally observed: an increase in the formation of paraffins from olefins and a decrease, over time on stream, in the low concentration of CO_2 at the reactor outlet. Figure 2d, which corresponds to the results obtained with the In_2O_3−ZrO_2 catalyst, shows the model's prediction without the deactivation effect of SAPO-34. The In_2O_3−ZrO_2 catalyst is only active for the rWGS and methanol synthesis reactions, in which the concentration is much lower compared to that in previous cases due to the absence of synergy with the oxygenate-to-olefin conversion step.

The deactivation kinetics of the SAPO-34 catalyst are of great importance in the kinetic model. Figure S6a illustrates the evolution of the calculated activity with the longitudinal position and time on stream under specific reaction conditions. The preferential deactivation at the reactor inlet and the progressive trend for higher reactor longitudinal positions are characteristic of the MTO process,[52,55] where coke is primarily formed through the adsorption of oxygenates as reactants on the acid sites, as described by the proposed kinetic eq (eq 27). In Figure S6b, it is observed that with the progression of

https://doi.org/10.1021/acssuschemeng.3c06914
ACS Sustainable Chem. Eng. 2024, 12, 1616−1624

deactivation, the normalized olefin yield tends to a stable value corresponding to the remnant activity of the catalyst.

Relating this result to the kinetic model, it can be observed that the decrease in activity and the increase in oxygenate (methanol) concentration, due to deactivation, have opposite effects on the evolution of normalized olefin formation rate over time on stream (eqs 16−18 in Table 1). Thus, the product of these two variables (Figure S6c) follows the same trend and explains Figure S6a.

Reactor Simulation. The model allows for analyzing the effect of temperature, pressure, and CO_2/CO_x ratio in the feed on the yield of light olefins, as well as on CO_2 and CO_x conversions. As an example, the results in Figure 3 correspond to the hydrogenation of an equimolar stream of CO and CO_2 using a catalyst with an In_2O_3−ZrO_2/SAPO-34 ratio of 2/1 under specific reaction conditions and at zero time on stream (fresh catalyst). Under such conditions, the maximum olefin yield exceeds 6% (Figure 3a) with a selectivity above 60%, CO_x conversion reaches 12% (Figure 3b) and CO_2 conversion accounts for 16% (Figure 3c) at 415 °C and 50 bar.

It is worth noting that the methodology used in the kinetic modeling, considering the activity and deactivation independently for each of the individual catalysts, allows for predicting the performance of the tandem catalyst at different catalyst loadings. Figure 4a shows that the olefin yield increases with

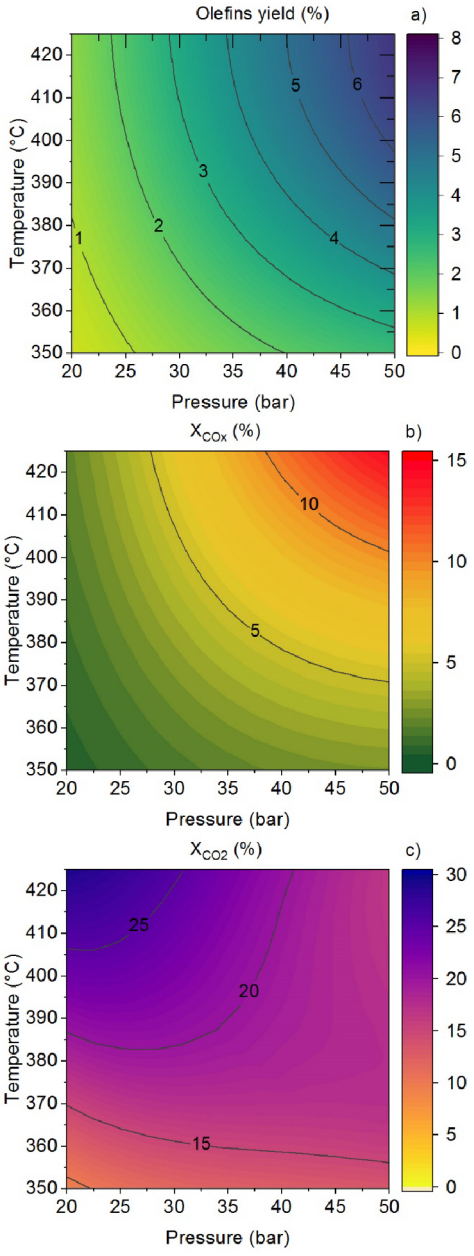

Figure 3. Prediction of the kinetic model on the effect of temperature and pressure on olefins yield (a), CO_x conversion (b), and CO_2 conversion (c). Reaction conditions: H_2/CO_x ratio in the feed, 3; CO_2/CO ratio in the feed, 0.5; space time, 5 g_{cat} h mol_C^{-1}, and ∼0 h on stream.

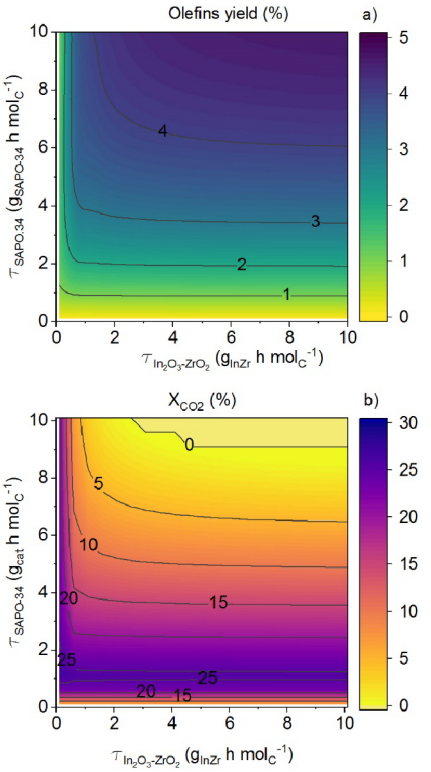

Figure 4. Prediction of the kinetic model on the effect of In_2O_3−ZrO_2 and SAPO-34 loadings on olefins yield (a) and CO_2 conversion (b). Reaction conditions: H_2/CO_x ratio in the feed, 3; CO_2/CO ratio in the feed, 0.5; 400 °C; ∼ 0 h on stream; 50 bar (a) and 30 bar (b).

higher space time values of the SAPO-34 catalyst. Moreover, the In_2O_3−ZrO_2/SAPO-34 ratio of 2 (corresponding to a line with slope 2) exhibits the steepest slope, indicating that it is the optimal ratio for boosting the olefin yield. Figure 4b depicts the CO_2 conversion for different space time values of each of the individual catalysts, showing a maximum CO_2 conversion at low SAPO-34 loadings (slightly above 1 $g_{SAPO-34}$ h mol_C^{-1}). This circumstance predicted by the model is a direct consequence of the effect of H_2O concentration in the medium (resulting from rWGS, methanol dehydration, and olefin formation reaction), as it hampers the rWGS reaction and leads to a complete blockage of the CO_2 conversion.

Based on the aforementioned results, aside from the significant benefit in terms of catalyst stability, the concentration of H_2O in the reaction medium is the main limiting factor for achieving high olefin yields when the SAPO-34 content in the tandem catalyst is high. As evidence of this, a simulation was conducted for an ideal system in which H_2O is

https://doi.org/10.1021/acssuschemeng.3c06914
ACS Sustainable Chem. Eng. 2024, 12, 1616−1624

immediately adsorbed. As shown in Figure 5a, the olefin yield surges to 17%, and complete CO_2 conversion is achieved

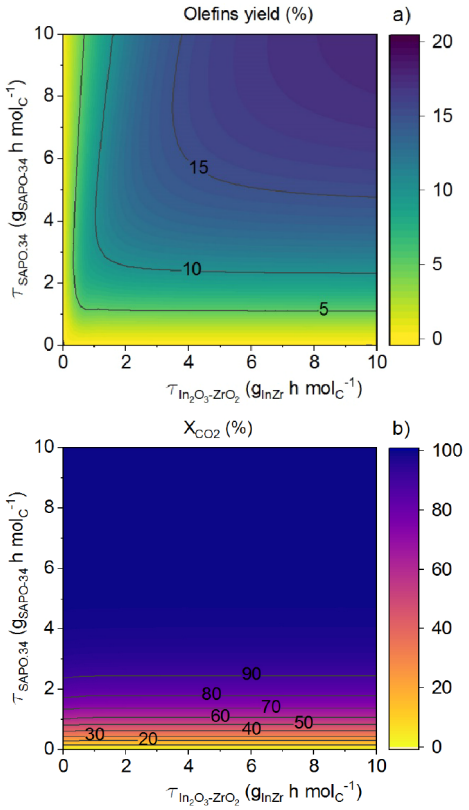

Figure 5. Prediction of the kinetic model on the effect of In_2O_3−ZrO_2 and SAPO-34 loadings on olefins yield (a) and CO_2 conversion (b) assuming complete and immediate H_2O removal. Reaction conditions: H_2/CO_x ratio in the feed, 3; CO_2/CO ratio in the feed, 0.5; 400 °C; 30 bar; and ∼0 h on stream.

(Figure 5b). Therefore, two main strategies are proposed for further study seeking industrial operating conditions that imply H_2O removal: a hydrophilic membrane reactor or *in situ* H_2O adsorption. The latter alternative would require more investment in equipment to ensure continuous operation, that is, parallel reactors connected to an adsorption−desorption system. It is worth mentioning that significant technological advancements have been made in other catalytic processes involving CO_2 valorization in the presence of H_2O, such as the direct DME synthesis, which employs hydrophilic membranes[56−58] or adsorption systems.[59]

CONCLUSIONS

The proposed kinetic model is based on a reaction network with 12 individual steps and adequately describes the performance of an In_2O_3−ZrO_2/SAPO-34 tandem catalyst in the direct production of light olefins through the hydrogenation of CO_2/CO mixtures. The model predicts the performance in terms of product distribution, CO_2 and CO_x conversions, and their evolution over time on stream within the 350−425 °C, 20−50 bar ranges, and a CO_2/CO_x ratio between 0 and 1. Considering the activity of each individual catalyst in the kinetic model allows the prediction of the performance of the tandem catalyst when prepared by physical mixing with different loadings of the individual catalysts. It is also noteworthy that the deactivation of the tandem catalyst is considered through kinetic equations for the deactivation of the individual catalysts, confirming that the deactivation of SAPO-34 is the main cause and the influence of methanol as a coke precursor and that of H_2O and H_2 concentrations as coke formation mitigating agents.

The model proves useful for optimizing process variables and predicts an olefin yield surpassing 6% (selectivity above 60%), a CO_x conversion of 12%, and a CO_2 conversion of 16% at 415 °C and 50 bar for a CO_2/CO_x ratio of 0.5 in the feed. Additionally, it quantifies the effect of the concentration of methanol, H_2O, and H_2 on the results, suggesting the opportunity to use a hydrophilic membrane reactor. Using this reactor, the model predicts an olefin yield of 17% and complete CO_2 conversion.

The availability of the proposed kinetic model is of significant interest for exploring the scale-up prospects of the process with catalysts utilizing In_2O_3−ZrO_3 and SAPO-34 in their configuration. Moreover, the fundamental aspects described in the development of the model will be useful for kinetic modeling with other OX/ZEO catalysts under development for the direct production of olefins and other hydrocarbons from CO_2/CO mixtures.

ASSOCIATED CONTENT

Supporting Information

The Supporting Information is available free of charge at https://pubs.acs.org/doi/10.1021/acssuschemeng.3c06914.

Catalysts' properties are provided in Section S1; experimental run conditions and reproducibility in Section S2; assessment of potential mass transfer limitation in Section S3; reaction indices defined in Section S4; the methodology for kinetic data analysis described in Section S5; and, further information regarding the fitting obtained with the model and simulation in Section S6 (PDF)

AUTHOR INFORMATION

Corresponding Author

Ainara Ateka − *Department of Chemical Engineering, University of the Basque Country UPV/EHU, Bilbao 48080, Spain;* orcid.org/0000-0002-3863-5808; Phone: +34-94-6015361; Email: ainara.ateka@ehu.eus

Authors

Ander Portillo − *Department of Chemical Engineering, University of the Basque Country UPV/EHU, Bilbao 48080, Spain*

Onintze Parra − *Department of Chemical Engineering, University of the Basque Country UPV/EHU, Bilbao 48080, Spain*

Andres T. Aguayo − *Department of Chemical Engineering, University of the Basque Country UPV/EHU, Bilbao 48080, Spain*

Javier Ereña − *Department of Chemical Engineering, University of the Basque Country UPV/EHU, Bilbao 48080, Spain*

Javier Bilbao − *Department of Chemical Engineering, University of the Basque Country UPV/EHU, Bilbao 48080, Spain;* orcid.org/0000-0001-7084-9665

Complete contact information is available at: https://pubs.acs.org/10.1021/acssuschemeng.3c06914

Notes

The authors declare no competing financial interest.

■ ACKNOWLEDGMENTS

This work has been carried out with the financial support of the Ministry of Science, Innovation and Universities of the Spanish Government (PID2022-140584OB-I00); the Basque Government (Project IT1645-22), the European Regional Development Funds (ERDF) and the European Commission (HORIZON H2020-MSCA RISE-2018. Contract No. 823745). A. Portillo is grateful for the Ph.D. grant from the Ministry of Science, Innovation and Universities of the Spanish Government (BES2017-081135). Onintze Parra is grateful for the financial support of the grant of the Basque Government (PRE_2021_1_0014).

■ REFERENCES

(1) Jiang, Y.; Wang, K.; Wang, Y.; Liu, Z.; Gao, X.; Zhang, J.; Ma, Q.; Fan, S.; Zhao, T.-S.; Yao, M. Recent Advances in Thermocatalytic Hydrogenation of Carbon Dioxide to Light Olefins and Liquid Fuels via Modified Fischer−Tropsch Pathway. *J. CO2 Util.* **2023**, *67*, 102321.

(2) Sharma, P.; Sebastian, J.; Ghosh, S.; Creaser, D.; Olsson, L. Recent Advances in Hydrogenation of CO_2 into Hydrocarbons via Methanol Intermediate over Heterogeneous Catalysts. *Catal. Sci. Technol.* **2021**, *11*, 1665−1697.

(3) Kamkeng, A. D. N.; Wang, M.; Hu, J.; Du, W.; Qian, F. Transformation Technologies for CO_2 Utilisation: Current Status, Challenges and Future Prospects. *Chem. Eng. J.* **2021**, *409*, 128138.

(4) Zhang, X.; Yuan, C.; Huang, Z.; Xu, H.; Shen, W. Recent Advances in Catalytic Hydrogenation of CO_2 into Value-Added Chemicals over Oxide−Zeolite Bifunctional Catalysts. *Catal. Today* **2023**, *422*, 114219.

(5) Zhang, W.; Wang, S.; Guo, S.; Qin, Z.; Dong, M.; Wang, J.; Fan, W. Effective Conversion of CO_2 into Light Olefins along with Generation of Low Amounts of CO. *J. Catal.* **2022**, *413*, 923−933.

(6) Ramirez, A.; Ticali, P.; Salusso, D.; Cordero-Lanzac, T.; Ould-Chikh, S.; Ahoba-Sam, C.; Bugaev, A. L.; Borfecchia, E.; Morandi, S.; Signorile, M.; Bordiga, S.; Gascon, J.; Olsbye, U. Multifunctional Catalyst Combination for the Direct Conversion of CO_2 to Propane. *JACS Au* **2021**, *1*, 1719−1732.

(7) Li, W.; Zhan, G.; Liu, X.; Yue, Y.; Tan, K. B.; Wang, J.; Huang, J.; Li, Q. Assembly of $ZnZrO_x$ and ZSM-5 on Hierarchically Porous Bio-Derived SiO_2 Platform as Bifunctional Catalysts for CO_2 Hydrogenation to Aromatics. *Appl. Catal., B* **2023**, *330*, 122575.

(8) Zhang, L.; Gao, W.; Wang, F.; Wang, C.; Liang, J.; Guo, X.; He, Y.; Yang, G.; Tsubaki, N. Highly Selective Synthesis of Light Aromatics from CO_2 by Chromium-Doped ZrO_2 Aerogels in Tandem with HZSM-5@SiO_2 Catalyst. *Appl. Catal., B* **2023**, *328*, 122535.

(9) Lu, P.; Liang, J.; Wang, K.; Liu, B.; Atchimarungsri, T.; Wang, Y.; Zhang, X.; Tian, J.; Jiang, Y.; Liu, Z.; Reubroycharoen, P.; Zhao, T.; Zhang, J.; Gao, X. Boosting Liquid Hydrocarbon Synthesis from CO_2 Hydrogenation via Tailoring Acid Properties of HZSM-5 Zeolite. *Ind. Eng. Chem. Res.* **2022**, *61*, 16393−16401.

(10) Parra, O.; Portillo, A.; Ereña, J.; Aguayo, A. T.; Bilbao, J.; Ateka, A. Boosting the Activity in the Direct Conversion of CO_2/CO Mixtures into Gasoline Using ZnO-ZrO_2 Catalyst in Tandem with HZSM-5 Zeolite. *Fuel Process. Technol.* **2023**, *245*, 107745.

(11) Ateka, A.; Rodriguez-Vega, P.; Ereña, J.; Aguayo, A. T.; Bilbao, J. A Review on the Valorization of CO_2. Focusing on the Thermodynamics and Catalyst Design Studies of the Direct Synthesis of Dimethyl Ether. *Fuel Process. Technol.* **2022**, *233*, 107310.

(12) Ateka, A.; Pérez-Uriarte, P.; Gamero, M.; Ereña, J.; Aguayo, A. T.; Bilbao, J. A Comparative Thermodynamic Study on the CO_2 Conversion in the Synthesis of Methanol and of DME. *Energy* **2017**, *120*, 796−804.

(13) Frei, M. S.; Mondelli, C.; Cesarini, A.; Krumeich, F.; Hauert, R.; Stewart, J. A.; Curulla Ferré, D.; Pérez-Ramírez, J. Role of Zirconia in Indium Oxide-Catalyzed CO_2 Hydrogenation to Methanol. *ACS Catal.* **2020**, *10*, 1133−1145.

(14) Azhari, N. J.; Erika, D.; Mardiana, S.; Ilmi, T.; Gunawan, M. L.; Makertihartha, I. G. B. N.; Kadja, G. T. M. Methanol Synthesis from CO_2: A Mechanistic Overview. *Results Eng.* **2022**, *16*, 100711.

(15) Niu, J.; Liu, H.; Jin, Y.; Fan, B.; Qi, W.; Ran, J. Comprehensive Review of Cu-Based CO_2 Hydrogenation to CH_3OH: Insights from Experimental Work and Theoretical Analysis. *Int. J. Hydrogen Energy* **2022**, *47*, 9183−9200.

(16) Yusuf, N.; Almomani, F. Highly Effective Hydrogenation of CO_2 to Methanol over Cu/ZnO/Al_2O_3 Catalyst: A Process Economy & Environmental Aspects. *Fuel* **2023**, *332*, 126027.

(17) Cordero-Lanzac, T.; Ramirez, A.; Navajas, A.; Gevers, L.; Brunialti, S.; Gandía, L. M.; Aguayo, A. T.; Mani Sarathy, S.; Gascon, J. A Techno-Economic and Life Cycle Assessment for the Production of Green Methanol from CO_2: Catalyst and Process Bottlenecks. *J. Energy Chem.* **2022**, *68*, 255−266.

(18) Bjørgen, M.; Svelle, S.; Joensen, F.; Nerlov, J.; Kolboe, S.; Bonino, F.; Palumbo, L.; Bordiga, S.; Olsbye, U. Conversion of Methanol to Hydrocarbons over Zeolite H-ZSM-5: On the Origin of the Olefinic Species. *J. Catal.* **2007**, *249*, 195−207.

(19) Ilias, S.; Bhan, A. Mechanism of the Catalytic Conversion of Methanol to Hydrocarbons. *ACS Catal.* **2013**, *3*, 18−31.

(20) Yarulina, I.; Chowdhury, A. D.; Meirer, F.; Weckhuysen, B. M.; Gascon, J. Recent Trends and Fundamental Insights in the Methanol-to-Hydrocarbons Process. *Nat. Catal.* **2018**, *1*, 398−411.

(21) Zhang, Q.; Yu, J.; Corma, A. Applications of Zeolites to C1 Chemistry: Recent Advances, Challenges, and Opportunities. *Adv. Mater.* **2020**, *32*, No. e2002927.

(22) Pérez-Uriarte, P.; Ateka, A.; Aguayo, A. T.; Gayubo, A. G.; Bilbao, J. Kinetic Model for the Reaction of DME to Olefins over a HZSM-5 Zeolite Catalyst. *Chem. Eng. J.* **2016**, *302*, 801−810.

(23) Ali, S. S.; Zaidi, H. A. Experimental and Kinetic Modeling Studies of Methanol Transformation to Hydrocarbons Using Zeolite-Based Catalysts: A Review. *Energy Fuels* **2020**, *34*, 13225−13246.

(24) Tan, K. B.; Xu, K.; Cai, D.; Huang, J.; Zhan, G. Rational Design of Bifunctional Catalysts with Proper Integration Manners for CO and CO_2 Hydrogenation into Value-Added Products: A Review. *Chem. Eng. J.* **2023**, *463*, 142262.

(25) Portillo, A.; Ateka, A.; Ereña, J.; Aguayo, A. T.; Bilbao, J. Conditions for the Joint Conversion of CO_2 and Syngas in the Direct Synthesis of Light Olefins Using In_2O_3−ZrO_2/SAPO-34 Catalyst. *Ind. Eng. Chem. Res.* **2022**, *61*, 10365−10376.

(26) Portillo, A.; Ateka, A.; Ereña, J.; Bilbao, J.; Aguayo, A. T. Role of Zr Loading into In_2O_3 Catalysts for the Direct Conversion of CO_2/CO Mixtures into Light Olefins. *J. Environ. Manage.* **2022**, *316*, 115329.

(27) Portillo, A.; Ateka, A.; Ereña, J.; Bilbao, J.; Aguayo, A. T. Alternative Acid Catalysts for the Stable and Selective Direct Conversion of CO_2/CO Mixtures into Light Olefins. *Fuel Process. Technol.* **2022**, *238*, 107513.

(28) Portillo, A.; Parra, O.; Ereña, J.; Aguayo, A. T.; Bilbao, J.; Ateka, A. Effect of Water and Methanol Concentration in the Feed on the Deactivation of In_2O_3-ZrO_2/SAPO-34 Catalyst in the Conversion of CO_2/CO to Olefins by Hydrogenation. *Fuel* **2023**, *346*, 128298.

(29) Portillo, A.; Parra, O.; Aguayo, A. T.; Ereña, J.; Bilbao, J.; Ateka, A. Setting up In_2O_3-ZrO_2/SAPO-34 Catalyst for Improving Olefin Production via Hydrogenation of CO_2/CO Mixtures. *Catalysts* **2023**, *13*, 1101.

(30) Ghosh, S.; Olsson, L.; Creaser, D. Methanol Mediated Direct CO_2 Hydrogenation to Hydrocarbons: Experimental and Kinetic Modeling Study. *Chem. Eng. J.* **2022**, *435*, 135090.

(31) Ghosh, S.; Sebastian, J.; Olsson, L.; Creaser, D. Experimental and Kinetic Modeling Studies of Methanol Synthesis from CO_2 Hydrogenation Using In_2O_3 Catalyst. *Chem. Eng. J.* **2021**, *416*, 129120.

https://doi.org/10.1021/acssuschemeng.3c06914
ACS Sustainable Chem. Eng. 2024, 12, 1616−1624

(32) Cordero-Lanzac, T.; Ramirez, A.; Cruz-Fernandez, M.; Zander, H.-J.; Joensen, F.; Woolass, S.; Meiswinkel, A.; Styring, P.; Gascon, J.; Olsbye, U. A CO_2 Valorization Plant to Produce Light Hydrocarbons: Kinetic Model, Process Design and Life Cycle Assessment. *J. CO2 Util.* **2023**, *67*, 102337.
(33) Cordero-Lanzac, T.; Martínez, C.; Aguayo, A. T.; Castaño, P.; Bilbao, J.; Corma, A. Activation of N-Pentane While Prolonging HZSM-5 Catalyst Lifetime during Its Combined Reaction with Methanol or Dimethyl Ether. *Catal. Today* **2022**, *383*, 320−329.
(34) Bonnin, A.; Pouilloux, Y.; Coupard, V.; Uzio, D.; Pinard, L. Deactivation Mechanism and Regeneration Study of Zn/HZSM-5 Catalyst in Ethylene Transformation. *Appl. Catal., A* **2021**, *611*, 117976.
(35) Levenspiel, O.. *Chemical Reaction Engineering*, 3rd ed.; John Wiley & Sons: New York, 1999.
(36) Cordero-Lanzac, T.; Aguayo, A. T.; Gayubo, A. G.; Castaño, P.; Bilbao, J. Simultaneous Modeling of the Kinetics for N-Pentane Cracking and the Deactivation of a HZSM-5 Based Catalyst. *Chem. Eng. J.* **2018**, *331*, 818−830.
(37) Gayubo, A. G.; Aguayo, A. T.; Sánchez Del Campo, A. E.; Tarrío, A. M.; Bilbao, J. Kinetic Modeling of Methanol Transformation into Olefins on a SAPO-34 Catalyst. *Ind. Eng. Chem. Res.* **2000**, *39*, 292−300.
(38) Pérez-Uriarte, P.; Ateka, A.; Gamero, M.; Aguayo, A. T.; Bilbao, J. Effect of the Operating Conditions in the Transformation of DME to Olefins over a HZSM-5 Zeolite Catalyst. *Ind. Eng. Chem. Res.* **2016**, *55*, 6569−6578.
(39) Cordero-Lanzac, T.; Ateka, A.; Pérez-Uriarte, P.; Castaño, P.; Aguayo, A. T.; Bilbao, J. Insight into the Deactivation and Regeneration of HZSM-5 Zeolite Catalysts in the Conversion of Dimethyl Ether to Olefins. *Ind. Eng. Chem. Res.* **2018**, *57*, 13689−13702.
(40) Zapater, D.; Lasobras, J.; Soler, J.; Herguido, J.; Menéndez, M. Comparison of Conventional and Two-Zone Fluidized Bed Reactors for Methanol to Olefins. Effect of Reaction Conditions and the Presence of Water in the Feed. *Ind. Eng. Chem. Res.* **2022**, *61*, 5757−5765.
(41) Arora, S. S.; Nieskens, D. L. S.; Malek, A.; Bhan, A. Lifetime Improvement in Methanol-to-Olefins Catalysis over Chabazite Materials by High-Pressure H_2 Co-Feeds. *Nat. Catal.* **2018**, *1*, 666−672.
(42) Nieskens, D. L. S.; Lunn, J. D.; Malek, A. Understanding the Enhanced Lifetime of SAPO-34 in a Direct Syngas-to-Hydrocarbons Process. *ACS Catal.* **2019**, *9*, 691−700.
(43) Zhao, X.; Li, J.; Tian, P.; Wang, L.; Li, X.; Lin, S.; Guo, X.; Liu, Z. Achieving a Superlong Lifetime in the Zeolite-Catalyzed MTO Reaction under High Pressure: Synergistic Effect of Hydrogen and Water. *ACS Catal.* **2019**, *9*, 3017−3025.
(44) Smith, J. M.; Van Ness, H. C.; Abbott, M. M.; Swihart, M. T.. *Introduction to Chemical Engineering Thermodynamics*; McGraw-Hill Education: New York, 2018.
(45) Ateka, A.; Portillo, A.; Sánchez-Contador, M.; Bilbao, J.; Aguayo, A. T. Macro-Kinetic Model for CuO−ZnO−ZrO_2@SAPO-11 Core-Shell Catalyst in the Direct Synthesis of DME from CO/CO_2. *Renewable Energy* **2021**, *169*, 1242−1251.
(46) Cordero-Lanzac, T.; Hita, I.; García-Mateos, F. J.; Castaño, P.; Rodríguez-Mirasol, J.; Cordero, T.; Bilbao, J. Adaptable Kinetic Model for the Transient and Pseudo-Steady States in the Hydrodeoxygenation of Raw Bio-Oil. *Chem. Eng. J.* **2020**, *400*, 124679.
(47) Pérez-Uriarte, P.; Ateka, A.; Gayubo, A. G.; Cordero-Lanzac, T.; Aguayo, A. T.; Bilbao, J. Deactivation Kinetics for the Conversion of Dimethyl Ether to Olefins over a HZSM-5 Zeolite Catalyst. *Chem. Eng. J.* **2017**, *311*, 367−377.
(48) Vela, F. J.; Palos, R.; Trueba, D.; Cordero-Lanzac, T.; Bilbao, J.; Arandes, J. M.; Gutiérrez, A. A Six-Lump Kinetic Model for HDPE/VGO Blend Hydrocracking. *Fuel* **2023**, *333*, 126211.
(49) Trueba, D.; Palos, R.; Bilbao, J.; Arandes, J. M.; Gutiérrez, A. Kinetic Modeling of the Hydrocracking of Polystyrene Blended with Vacuum Gasoil. *Chem. Eng. J.* **2023**, *451*, 138709.
(50) Guisnet, M.; Magnoux, P. Organic Chemistry of Coke Formation. *Appl. Catal., A* **2001**, *212*, 83−96.
(51) Ibáñez, M.; Pérez-Uriarte, P.; Sánchez-Contador, M.; Cordero-Lanzac, T.; Aguayo, A. T.; Bilbao, J.; Castaño, P. Nature and Location of Carbonaceous Species in a Composite HZSM-5 Zeolite Catalyst during the Conversion of Dimethyl Ether into Light Olefins. *Catalysts* **2017**, *7*, 254.
(52) Aguayo, A. T.; Campo, A. E. S. d.; Gayubo, A. G.; Tarrío, A.; Bilbao, J. Deactivation by Coke of a Catalyst Based on a SAPO-34 in the Transformation of Methanol into Olefins. *J. Chem. Technol. Biotechnol.* **1999**, *74*, 315−321.
(53) Chen, J.; Li, J.; Wei, Y.; Yuan, C.; Li, B.; Xu, S.; Zhou, Y.; Wang, J.; Zhang, M.; Liu, Z. Spatial Confinement Effects of Cage-Type SAPO Molecular Sieves on Product Distribution and Coke Formation in Methanol-to-Olefin Reaction. *Catal. Commun.* **2014**, *46*, 36−40.
(54) Luo, M.; Hu, B.; Mao, G.; Wang, B. Trace Compounds Confined in SAPO-34 and a Probable Evolution Route of Coke in the MTO Process. *ACS Omega* **2022**, *7*, 3277−3283.
(55) Müller, S.; Liu, Y.; Vishnuvarthan, M.; Sun, X.; van Veen, A. C.; Haller, G. L.; Sanchez-Sanchez, M.; Lercher, J. A. Coke Formation and Deactivation Pathways on H-ZSM-5 in the Conversion of Methanol to Olefins. *J. Catal.* **2015**, *325*, 48−59.
(56) Rodriguez-Vega, P.; Ateka, A.; Kumakiri, I.; Vicente, H.; Ereña, J.; Aguayo, A. T.; Bilbao, J. Experimental Implementation of a Catalytic Membrane Reactor for the Direct Synthesis of DME from H_2+CO/CO_2. *Chem. Eng. Sci.* **2021**, *234*, 116396.
(57) Ateka, A.; Rodriguez-Vega, P.; Cordero-Lanzac, T.; Bilbao, J.; Aguayo, A. T. Model Validation of a Packed Bed LTA Membrane Reactor for the Direct Synthesis of DME from CO/CO_2. *Chem. Eng. J.* **2021**, *408*, 127356.
(58) Ateka, A.; Rodriguez-Vega, P.; Ereña, J.; Aguayo, A. T.; Bilbao, J. Kinetic Modeling and Reactor Design of the Direct Synthesis of Dimethyl Ether for CO_2 Valorization. A Review. *Fuel* **2022**, *327*, 125148.
(59) Bayat, M.; Asil, A. G. Efficient In-Situ Water Adsorption for Direct DME Synthesis: Robust Computational Modeling and Multi-Objective Optimization. *J. Nat. Gas Sci. Eng.* **2020**, *83*, 103587.

https://doi.org/10.1021/acssuschemeng.3c06914
ACS Sustainable Chem. Eng. 2024, 12, 1616−1624